Journal of Materials Chemistry A

ROYAL SOCIETY OF CHEMISTRY

COMMUNICATION

View Article Online
View Journal | View Issue

Cite this: J. Mater. Chem. A, 2026, 14, 13346

Received 8th December 2025
Accepted 19th March 2026

DOI: 10.1039/d5ta10019d

rsc.li/materials-a

Dual-carbon batteries using fluorination and defluorination reactions

Yuta Ito, [ab] Changhee Lee, *[ac] Yuto Miyahara, [a] Takeshi Abe [a] and Kohei Miyazaki *[ad]

Dual-carbon batteries (DCBs) employing carbon-based electrodes are promising next-generation systems but suffer from limited capacity due to bulky anions and electrolyte instability during simultaneous (de) intercalation. Here, we demonstrate a new class of fluorination-based DCBs utilizing LiF as an F^- source, paired with graphite anodes and Li-based concentrated sulfolane electrolytes for high-voltage operation. The system delivers a large initial reversible capacity of 356 mAh g^{-1} (per cathode carbon) and exhibits notable capacity retention, outperforming conventional DCB systems. Air-free X-ray diffraction analyses reveal that reversible electrochemical utilization of LiF, suppression of LiF crystallite growth, optimized carbon crystallite size, LiF retention on carbon cathodes, and restrained electrolyte decomposition collectively enable large capacity and stable cycling. These findings establish the first fluorination/defluorination-based DCBs as a feasible next-generation battery technology using the smallest ions (Li^+ and F^-) to achieve high energy density and cycling durability.

Introduction

The growing demand for rechargeable energy storage systems has accelerated the advancement of battery technologies. Despite their market dominance, lithium-ion batteries (LIBs) face challenges associated with the mining and refinement of critical raw materials, *e.g.*, cobalt and nickel, and electrochemical performance limitations, including energy density and cycle life. These issues raise concerns regarding the long-term sustainability, cost competitiveness, and supply security of LIBs, particularly for large-scale transportation and stationary energy storage.

As a promising alternative for next-generation battery systems, dual-carbon batteries (DCBs) utilize carbonaceous active materials for both cathodes and anodes, respectively, with simultaneous cation and anion (de)insertion into the respective electrodes. High operating potentials for anion uptake (>4.5 V *vs.* Li^+/Li), low thermal runaway risk, and abundant carbon materials make them attractive compared to LIBs with transition metal oxide cathodes.[1–5] Since 1994, when Carlin *et al.* first proposed DCBs using 1-ethyl-3-methylimidazolium (EMI^+) or 1,2-dimethyl-3-propylimidazolium ($DMPI^+$) as cations and $AlCl_4^-$, BF_4^-, PF_6^-, $CF_3SO_3^-$, or $C_6H_5CO_2^-$ as anions for graphite anodes/cathodes,[6] this concept has been expanded to systems utilizing Li^+ intercalation as the anode reaction.[7] In particular, Seel *et al.* demonstrated PF_6^- intercalation in a Li/graphite half-cell, where the graphite cathode exhibited a capacity of ~100 mAh g^{-1} when charged to 5.45 V (*vs.* Li^+/Li).[8]

Meanwhile, conventional DCBs face challenges from their large anions, *e.g.*, PF_6^-,[8] BF_4^-,[9] ClO_4^-,[10] bis(trifluoromethanesulfonyl) amide ($TFSA^-$),[11] and bis(fluorosulfonyl)amide (FSA^-),[12] as guest anions at the cathode. These large anions inherently restrict the achievable reversible capacities and induce significant volume changes within the electrodes, resulting in severe capacity fading over repeated charge/discharge cycles. Furthermore, the fundamental reaction mechanism of DCBs entails the simultaneous (de)insertion of both cations and anions, which causes pronounced fluctuations in the electrolyte concentration and ionic conductivity during cycling. These fluctuations critically limit the achievable energy density of full-cell DCBs, which require a large electrolyte volume to buffer concentration changes and sustain ionic conductivity during operation (Fig. 1a).[2–4] Therefore, recent studies have used smaller anions, which have substantially improved the capacity of graphite cathodes. Yang *et al.* reported a BrCl intercalation reaction using LiCl–LiBr–graphite composite cathode, exhibiting a high reversible capacity of ~620 mAh g^{-1} within the range of 4.0–4.5 V (*vs.* Li^+/Li) to form $C_{3.5}[Br_{0.5}Cl_{0.5}]$.[13] Similarly, Guo *et al.* demonstrated an ICl

[a]Graduate School of Engineering, Kyoto University, Kyoto-shi Nishikyo-ku Katsura 615-8510, Japan. E-mail: lee@rs.tus.ac.jp; myzkohei@port.kobe-u.ac.jp

[b]Research Institute of Electrochemical Energy, Department of Energy and Environment, National Institute of Advanced Industrial Science and Technology (AIST), 1-8-31 Midorioka, Ikeda, Osaka 563-8577, Japan

[c]Department of Applied Chemistry, Tokyo University of Science, Shinjuku, Tokyo 162-8601, Japan

[d]Graduate School of Engineering, Kobe University, 1-1 Rokkodai, Nada, Kobe 657-8501, Japan

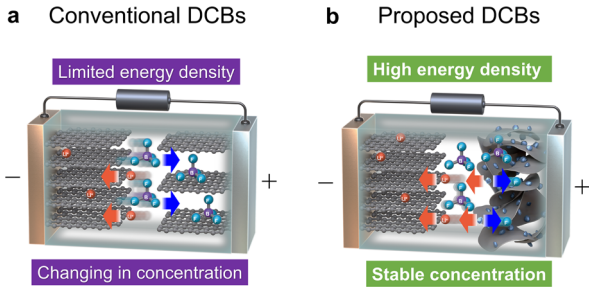

Fig. 1 Schematics of (a) conventional DCB and (b) the new proposed class of DCBs.

intercalation system achieving a capacity of ~291 mAh g^{-1} at 1.4 V (*vs.* the standard hydrogen electrode).[14] Kim *et al.* explored $LiCl_2$ superhalogen species as small anion intercalants to enhance DCB electrochemical performance.[15]

Our group has used even smaller F^- anions to improve performance.[16,17] As the fluorination potential on carbon cathodes is the highest among halogens and the theoretical capacity reaches 2231 mAh g^{-1} through the formation of $C_{1.0}F_{1.0}$, the fluorination reaction and Li^+ intercalation are together expected to maximize the energy density of DCBs. Specifically, we demonstrated the reversible insertion/de-insertion of F^- anions into/from graphite fluoride (CF_x) cathodes at suitably high potentials (up to 5.3 V *vs.* Li^+/Li).[16] LiF and carbon are generated *via* the electrochemical defluorination of CF_x, serving as the F-source and host material, respectively, at the cathode. Additionally, *operando* Raman spectroscopy revealed for the first time the electrochemical formation of a F^-–graphite intercalation compound (GIC), showing that artificial LiF coatings on graphite electrodes enhance F^- intercalation.[17] In addition, a recent study demonstrated that graphite-LiF mixed electrodes exhibit large reversible capacities in concentrated $LiBF_4$/sulfolane electrolytes due to fluorination/defluorination-assisted by inserted BF_4^-, further highlighting the potential of LiF-based carbon composites as high-performance positive electrodes for DCB systems.[18]

Here, we advance DCB concept by employing a graphite anode, a Li-based organic electrolyte, and LiF@carbon cathode electrochemically derived from CF_x. Distinct from both conventional bulky-anion DCBs and rechargeable Li/CF_x systems, our metal-free DCB architecture couples fluorination/defluorination *via* LiF as a F^- source to drive reversible (de) fluorination at the carbon cathode while maintaining Li^+ (de) intercalation at the graphite anode (Fig. 1b). By utilizing the smallest ionic pair (Li^+/F^-) and tuning LiF@carbon nanostructures, this design mitigates the anion size and electrolyte-concentration limitations of conventional DCBs[19] while eliminating the need for Li metal and thereby offering improved sustainability and enhanced safety compared with rechargeable Li/CF_x systems.

Results and discussion

First, composite cathodes consisting of LiF and carbon (xLiF@carbon) were prepared *via* the electrochemical defluorination of CF_x (eqn (1)).

$$CF_x + xLi^+ + xe^- \rightarrow C + xLiF \quad (1)$$

The electrochemical formation of xLiF@carbon was confirmed by analyzing discharge profiles (Fig. S1) and X-ray diffraction (XRD) measurements (Fig. S2). Notably, increasing the fluorine content from $CF_{0.52}$ to $CF_{1.0}$ enhanced the defluorination capacity, confirming the electrochemical defluorination reaction described by eqn (1) and the formation of xLiF@carbon composites. Subsequently, DCBs were fabricated using the synthesized xLiF@carbon composites as cathodes and graphite anodes (Fig. S3).

Fig. 2 presents the charge/discharge curves and cycling performance for these DCBs, and the cyclability and initial discharge capacities both depended on the LiF content. Specifically, full cells with the 0.52LiF@carbon or 1.0LiF@carbon composite cathode and graphite anodes in 1 M $LiBF_4$ in ethylene carbonate and dimethyl carbonate (EC + DMC; 1 : 1 v/v) exhibited initial discharge capacities of 182 mAh per (g-carbon cathode) and 238 mAh per (g-carbon cathode), respectively (Fig. 2a and b). These cells experienced 70% and 39% capacity losses during cycling, respectively.

Notably, employing the concentrated sulfolane-based electrolyte dramatically enhanced both the capacity and the cycling stability (Fig. 2c–e): the capacity rapidly increased from 206 to 350 mAh g^{-1} within the first 10 cycles and was maintained at 330 mAh g^{-1} with only ~7.4% decay over 50 cycles. The coulombic efficiency (CE) was approximately 80% after 50 cycles (Fig. 2e), which is consistent with previously reported LiF-carbon conversion systems,[16–18,20] where CE values are generally limited by the intrinsic characteristics of the conversion chemistry.

In the present system, CE loss arises from both electrodes. On the anode side, the concentrated $LiBF_4$/sulfolane electrolyte

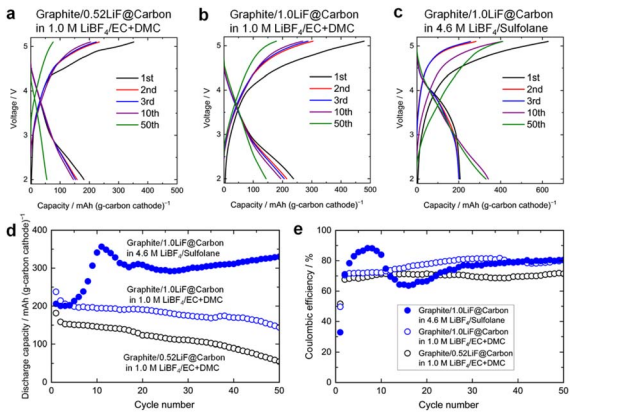

Fig. 2 Charge/discharge profiles of (a) graphite/0.52LiF@carbon and (b) graphite/1.0LiF@carbon full DCB cells in 1 M $LiBF_4$/EC + DMC at a current density of 200 mA per g (carbon cathode) within a voltage range of 2–5.1 V and charge/discharge profiles of (c) graphite/1.0LiF@carbon full DCB cells in 4.6 M $LiBF_4$/sulfolane at a current density of 50 mA per g (carbon cathode) within a voltage range of 2–5.1 V. The carbon cathode weights were calculated from the capacities of the electrochemical defluorination of CF_x; the calculation method is detailed in the SI. (d) Discharge capacity retention and (e) coulombic efficiency.

forms a comparatively less robust and continuously evolving SEI,[21] leading to Li^+ consumption during the early cycles until a sufficiently stable interphase is established. On the cathode side, the limited reversibility of the LiF decomposition/formation reaction[16–18,20] further constrains CE and becomes the dominant factor, which will be discussed later in more details. In addition, minor oxidative reactions at the high cut-off voltage (5.1 V) remain unavoidable, even with the expanded oxidative stability window offered by the concentrated electrolyte.

At the same time, the strong Li^+–BF_4^- interactions in the concentrated sulfolane electrolyte suppress BF_4^- intercalation and carbon degradation,[21] thereby mitigating irreversible LiF loss (to be discussed later). These combined effects enable the significant improvements in capacity and cycling stability, even under the high charging cutoff of 5.1 V. Further optimization of cell components, including the negative-to-positive electrode ratio, electrolyte-to-capacity ratio, electrode fabrication conditions, and separator design, remains a promising route to improving CE without compromising the demonstrated capacity and durability.

To understand the reaction mechanism of the proposed DCBs, cathode structural changes during charge/discharge were investigated by air-free *ex situ* XRD. The XRD pattern of $CF_{1.0}$ before the defluorination pre-treatment (Fig. 3a) exhibits three peaks at 12.7° ($d = 0.696$ nm), corresponding to $(C_2F)_n(002)$ and $(CF)_n(001)$; 25.7° ($d = 0.346$ nm) for carbon(002); and 41.0° ($d = 0.221$ nm) indicating $(C_2F)_n(101)$.[16] $CF_{1.0}$ and $CF_{0.52}$ show almost identical d values related to the graphite fluoride peak (Fig. S4), but $CF_{1.0}$ is more fluorinated than $CF_{0.52}$, and $CF_{1.0}$ has a less intense carbon (002) peak than $CF_{0.52}$, which is related to its large capacity. After defluorination (Fig. 3a), a broad peak appeared at ~21.5° ($d = 0.4171 \pm 0.0017$ nm), assigned to an intermediate compound, $C\{S_y \cdot xLi^+\}xF^-$, formed by Li^+ and solvent (S) co-intercalation into CF_x during discharge.[22–27] Furthermore, an additional broad carbon peak at ~25.7° and peaks for LiF(111) and (200) appeared, indicating that the intermediate partially decomposed, and the 1.0LiF@carbon composite formed. During the cycling of DCBs in conventional electrolytes, the peak shifts were caused by the expansion and contraction of carbon (002) (25.1–25.7°) due to anion insertion/de-insertion (Fig. 3b). However, because carbon may show low crystallinity or amorphous properties with less sp^2 content,[21] the interlayer distance and number of GIC stages could not be determined. Moreover, the relative intensity ratio of LiF(111) and carbon(002) (I_{LiF}/I_C) decreased after charging and increased after discharge (Fig. 3c), suggesting that fluorination/defluorination and decomposition/reformation of LiF reversibly occur during charge/discharge. Although obtained in 1 M $LiPF_6$/EC + DMC, charge/discharge behavior in Fig. S5 and change in the C 1s and F 1s signals shown in Fig. S6 indicate the reversible formation and decomposition of C–F bonds, providing additional support for the (de)fluorination mechanism.

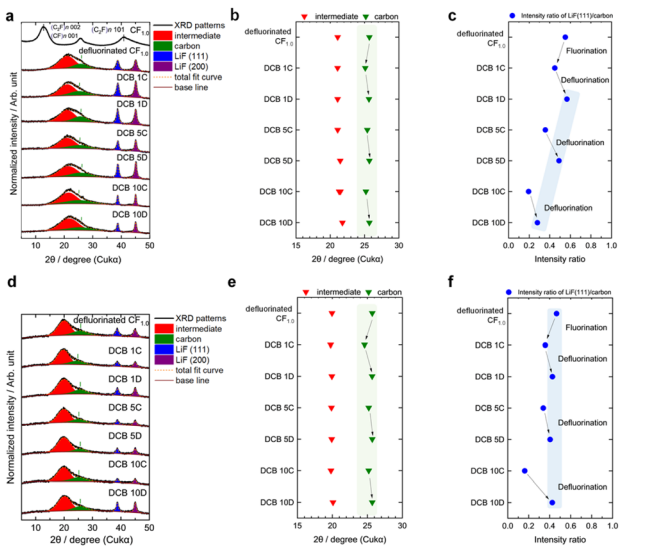

Fig. 3 (a and d) XRD patterns of LiF@carbon composite cathodes in DCBs at various states, (b and e) peak positions (2θ) of the intermediate and carbon, and (c and f) relative intensity ratio of LiF(111) *versus* carbon for the systems using (a–c) 1.0 M $LiBF_4$/EC + DMC or (d–f) 4.6 M $LiBF_4$/sulfolane ("defluorinated $CF_{1.0}$": pristine 1.0LiF@carbon composite cathodes; "DCB 1C–10D": after 1st charge–10th discharge of DCBs).

In contrast, the *ex situ* XRD patterns of the 1.0LiF@carbon electrodes tested in concentrated sulfolane-based electrolytes (Fig. 3d) demonstrated a peak for the intermediate at 20° (Fig. 3e). Compared with that of the conventional electrolyte system, the d spacing of the intermediate ($d = 0.4461 \pm 0.0009$ nm) increased because of solvent and concentration differences. Peak shifts caused by the expansion and contraction of carbon (002) (24.6–25.7°) due to anion insertion/de-insertion were similarly confirmed (Fig. 3e). Notably, I_{LiF}/I_C significantly increased from the 10th charge to the 10th discharge (DCBs 10C → DCBs 10D; Fig. 3f), indicating improved reactivity in fluorination/de-fluorination process. This enhancement corresponds to the increased discharge capacity at low voltages (2–3 V) observed during cycles 5–10 (Fig. 2c), suggesting that the apparent activation behavior may arise from the gradual stabilization of the graphite anode (as discussed later) together with the increased utility of the LiF at the cathode both of which requires several cycles to achieve fully stable intercalation reactions.

Furthermore, I_{LiF}/I_C did not decrease through cycle 10, indicating that the LiF loss was successfully suppressed during cycling, improving the cycling performance.

Furthermore, Fig. 4a and b show the crystallite sizes of LiF, carbon and intermediate in 1.0LiF@carbon during cycling estimated using the Scherrer eqn (2).

$$D = \frac{K\lambda}{B\cos\theta} \quad (2)$$

Table 1 Comparison of dual-carbon battery systems employing bulky anions in organic electrolytes and the Li^+/F^--based fluorination/defluorination dual-carbon battery proposed in this work

Electrolyte	Cathode	Anode	Potential (V)	Capacity [mAh per g (carbon)]	Ref.
4.6 M $LiBF_4$/sulfolane (SL)	LiF@carbon : AB : PVdF = 90 : 10 : 10	Natural graphite : PVdF = 90 : 10	1.5–5.1 V	356@0.05 A g^{-1}	This work
3.0 M $LiPF_6$/EMC	Al_2O_3@graphite : super P : CMC = 90 : 5 : 5	Graphite : super P : CMC = 90 : 5 : 5	3.0–5.0 V	80@0.5 A g^{-1}	32 (Li *et al.*, 2025)
3.0 M LiFSA/FEC + FEMC (3 : 7)	Graphite : AB : PAA = 85 : 5 : 10	Graphite : AB : PAA = 85 : 5 : 10	3.0–5.1 V	95@0.2 A g^{-1}	33 (Zhao *et al.*, 2023)
4.0 M $LiPF_6$/EMC	DTPMP@natural graphite : super P : PVdF = 80 : 10 : 10	Natural graphite : super P : CMC : SBR = 96 : 2 : 1 : 1	3.0–5.0 V	90@0.1 A g^{-1}	34 (Zhang *et al.*, 2023)
1 M $LiPF_6$/EMC + SL (1 : 4)	LTO@MCMB : super P : CMC = 90 : 5 : 5	MCMB : super P : CMC = 90 : 5 : 5	3.0–5.4 V	86.9@0.05 A g^{-1}	35 (Han *et al.*, 2019)
2 M $LiPF_6$/EMC + 3% VC	Graphite : super P : Alg = 80 : 10 : 10	Graphite : super P : Alg = 80 : 10 : 10	3.0–5.2 V	99.4@1 A g^{-1}	36 (Wang *et al.*, 2018)

(where D crystallite size (nm), K: Scherrer constant (0.89), λ: X-ray wavelength 0.15418 (nm), B: FWHM (rad), and θ: Bragg angle (rad)). Because of the high lattice energy of LiF, its crystal size may significantly affect the fluorination reactivity.[28] In 1 M $LiBF_4$/EC + DMC (the dilute electrolyte), the LiF crystallite size after the defluorination pre-treatment (1.0LiF@carbon formation) was estimated to be 8.4 nm, consistent with previous findings on the discharge mechanisms of CF_x.[24,29] After 10 cycles, the LiF crystallite size increased from 8.4 to 14 nm (Fig. 4). In contrast, in the 4.6 M $LiBF_4$/sulfolane electrolyte, the initial LiF crystallites were smaller (6.8 nm), and they grew more moderately during cycling to only 11 nm after 10 cycles (Fig. 4). Thus, the concentrated electrolyte suppressed LiF crystal growth (+58%) more effectively than the dilute one (+72%), indicating the improved reversibility of the fluorination/defluorination reactions. The smaller LiF crystallites in the sulfolane-based electrolyte likely contributed to the higher capacity, and the improved capacity retention may reflect suppressed crystallite growth. Furthermore, the carbon crystallites were on average 1.05 ± 0.07 and 1.50 ± 0.06 nm in the dilute and concentrated systems, respectively (Fig. 4). The intermediate compounds were also larger in the concentrated system on average. Therefore, achieving larger capacities and stable cyclability for fluorination/defluorination reactions may require smaller LiF crystallites and larger carbon crystallites in the cathode, enhancing the utilization of the LiF@carbon composites.

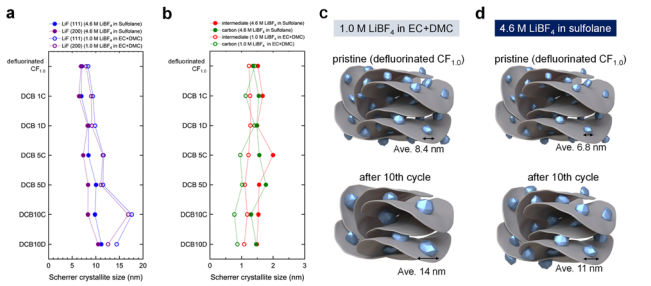

Fig. 4 Variations in Scherrer crystallite size (nm) of (a) LiF (blue: (111); purple: (200)) and (b) intermediate (red) and carbon (green), obtained from the air-free *ex situ* XRD of cathodes in DCBs using dilute 1.0 M $LiBF_4$/EC + DMC or concentrated 4.6 M $LiBF_4$/sulfolane. (c and d) Illustrations of 1.0LiF@carbon cathodes of pristine (after defluorination pre-treatment) and after cycle 10 in DCBs (DCB 10D) using (c) 1.0 M LiBF4/EC + DMC and 4.6 M $LiBF_4$/sulfolane.

Li^+ intercalation into the graphite anodes was also investigated by air-excluded *ex situ* XRD (Fig. S7). As this study focused on evaluating the feasibility of fluorination-based cathode reactions in DCBs and investigating the feasibility of the system, the N/P ratio was set excessively high (1.6–2.3). Using a graphite anode in the concentrated $LiBF_4$/sulfolane electrolyte requires a large amount of charge for SEI formation, decreasing the initial coulombic efficiency.[21] Therefore, Li–GIC formation on the anode side could not be confirmed in cycle 1. However, from cycle 5 onward, peaks appeared at 12°, 25.4°, and 54° in subsequent cycles, corresponding to stage-2 Li–GIC with a sandwich distance (d_s) of 0.700 nm.[30,31] These results indicate the feasibility of practically realizing fluorination-reaction-based DCB systems under the investigated conditions. Notably, even after an SEI sufficiently robust to enable reversible Li^+ intercalation/deintercalation is formed over the first few cycles, the overall CE remains limited to ~80% because the fluorination/defluorination reaction based on LiF decomposition/formation at the cathode does not proceed with high reversibility. In summary, the combination of LiF@carbon cathodes prepared from Li–$CF_{1.0}$ and graphite anodes enables a new DCB system, and the concentrated $LiBF_4$/sulfolane electrolyte ensures high capacity and cycling durability through enhanced oxidative stability and favorable LiF@carbon nanostructures. A brief comparison of representative DCB systems is summarized in Table 1. Compared with previously reported DCBs using bulky anions allow high-voltage operation yet suffer from restricted capacities,[32–36] and the present fluorination/defluorination architecture employing the smallest ionic pair, Li^+/F^-, uniquely enables both high capacity and high-voltage operation.

Conclusions

In conclusion, DCBs using Li^+ (de)intercalation into graphite anodes and (de)fluorination on cathodes were proposed as

a new type of rechargeable battery with low cost, high safety, and superior energy density. This system also provided a promising solution for the problems with conventional DCBs, *e.g.*, changes in the electrolyte concentration and the limited energy densities by using fluorination/defluorination reactions through LiF as the F source in the cathodes. Using the $CF_{1.0}$ cathode in 1 M $LiBF_4$/EC + DMC increased the capacity because it contained more LiF content than $CF_{0.52}$, although both systems suffered from capacity fading during cycling. In contrast, employing a concentrated $LiBF_4$/sulfolane electrolyte effectively suppressed side reactions at the cathode and promoted fluorination reaction, improving the capacity and cycling stability. Structural analysis revealed that the LiF and carbon crystallite sizes play a decisive role in the electrochemical performance, *e.g.*, cyclability and reversible capacities. Particularly, in the concentrated electrolyte for high-voltage operation, smaller LiF and larger carbon crystallites enhanced the capacity, while suppressed LiF crystallite growth correlated with superior cycling stability. These findings highlight the critical role of LiF and carbon nanostructures in achieving reversible fluorination/defluorination reactions. Overall, this study provides a foundation for developing advanced carbon cathodes based on (de)fluorination reactions, paving the way toward practical DCBs and other high-energy-density, long-life energy storage systems. Future work will focus on optimizing fluorination-based DCB configurations, decreasing the overpotential, and designing electrolytes tailored for stability and performance.

Author contributions

Y. I.: methodology; investigation (electrode fabrication, electrochemical measurements, XRD, XPS); data curation; formal analysis; visualization; writing – original draft. C. L.: conceptualization; methodology; data curation; visualization; writing – review & editing; supervision. Y. M.: writing – review & editing; supervision. T. A.: writing – review & editing; supervision. K. M.: conceptualization; methodology; data curation; visualization; writing – review & editing; supervision. All authors discussed the results, contributed to manuscript revision, and approved the final version.

Conflicts of interest

The authors declare no conflicts of interest.

Data availability

Data for this article, including the processed datasets and figures supporting the reported results, are available in the supplementary information (SI). Additional raw data and analysis scripts generated during this study are available from the corresponding author upon reasonable request. Supplementary information: Experimental section, discharge profiles of Li/CF_x cells in $LiBF_4$-based electrolytes, charge–discharge profiles and *ex situ* XRD patterns of Li/$CF_{0.52}$ half-cells using $LiPF_6$- and $LiBF_4$-based electrolytes, schematic procedure for the preparation of the proposed DCBs, cycling performance of the proposed DCBs (graphite/0.52LiF@carbon) in 1 M $LiPF_6$ electrolytes with different cutoff voltage ranges, XRD and XPS analyses of $CF_{0.52}$ before and after Li/$CF_{0.52}$ discharge, and of 0.52LiF@carbon cathodes and graphite anodes in assembled DCBs before and after charge. XRD patterns of $CF_{0.52}$ and $CF_{1.0}$ before electrochemical treatment, and air-free *ex situ* XRD patterns of graphite anodes in cycled graphite/1.0LiF@carbon DCBs using 4.6 M $LiBF_4$/sulfolane. See DOI: https://doi.org/10.1039/d5ta10019d.

Acknowledgements

This work was supported by JSPS KAKENHI (grant numbers 24K17777, 24K17772, and 24K01604) and JST FOREST Program (grant number JPMJFR2121). Additional financial support was partially provided by the Noguchi Institute.

References

1 M. Tebyetekerwa, T. T. Duignan, Z. Xu and X. Song Zhao, Rechargeable Dual-Carbon Batteries: A Sustainable Battery Technology, *Adv. Energy Mater.*, 2022, **12**(44), 2202450, DOI: 10.1002/aenm.202202450.

2 S. Chen, Q. Kuang and H. J. Fan, Dual-Carbon Batteries: Materials and Mechanism, *Small*, 2020, **16**(40), e2002803, DOI: 10.1002/smll.202002803.

3 Z. Guo, Z. Xu, F. Xie, J. Feng and M. Titirici, Strategies for High Energy Density Dual-Ion Batteries Using Carbon-Based Cathodes, *Adv. Energy Sustain. Res.*, 2021, **2**(11), 2100074, DOI: 10.1002/aesr.202100074.

4 M. Wang and Y. A Tang, Review on the Features and Progress of Dual-Ion Batteries, *Adv. Energy Mater.*, 2018, **8**(19), 1703320, DOI: 10.1002/aenm.201703320.

5 Y. Matsuo, A. Inoo and J. Inamoto, Electrochemical Intercalation Of Anions Into Graphite: Fundamental Aspects, Material Synthesis, and Application to The Cathode Of Dual-ion Batteries, *ChemistryOpen*, 2024, **13**(8), e202300244, DOI: 10.1002/open.202300244.

6 R. T. Carlin, H. C. De Long, J. Fuller and P. C. Trulove, Dual Intercalating Molten Electrolyte Batteries, *J. Electrochem. Soc.*, 1994, **141**(7), 73–76, DOI: 10.1149/1.2055041.

7 R. Santhanam and M. Noel, Effect of Solvents on the Intercalation/De-Intercalation Behaviour of Monovalent Ionic Species from Non-Aqueous Solvents on Polypropylene-Graphite Composite Electrode, *J. Power Sources*, 1997, **66**(1–2), 47–54, DOI: 10.1016/S0378-7753(96)02472-X.

8 J. A. Seel and J. R. Dahn, Electrochemical Intercalation of PF_6^- into Graphite, *J. Electrochem. Soc.*, 2000, **147**(3), 892–898, DOI: 10.1149/1.1393288.

9 L. Zhang, J. Li, Y. Huang, D. Zhu and H. Wang, Synergetic Effect of Ethyl Methyl Carbonate and Trimethyl Phosphate on BF_4^- Intercalation into a Graphite Electrode, *Langmuir*, 2019, **35**(11), 3972–3979, DOI: 10.1021/acs.langmuir.9b00262.

10 M. V. Gorbunov and D. Mikhailova, Peculiarities in Structural Behaviour of Graphite During Anionic Intercalation of PF_6^-, FSI^- and ClO_4^- at Elevated Temperature, *Chem. Commun.*, 2025, **61**(29), 5451–5454, DOI: 10.1039/d5cc00366k.

11 S. Rothermel, P. Meister, G. Schmuelling, O. Fromm, H.-W. Meyer, S. Nowak, M. Winter and T. Placke, Dual-Graphite Cells Based on the Reversible Intercalation of Bis(Trifluoromethanesulfonyl)Imide Anions from an Ionic Liquid Electrolyte, *Energy Environ. Sci.*, 2014, **7**(10), 3412–3423, DOI: 10.1039/c4ee01873g.

12 T. Fukutsuka, F. Yamane, K. Miyazaki and T. Abe, Electrochemical Intercalation of Bis(fluorosulfonyl)amide Anion into Graphite, *J. Electrochem. Soc.*, 2015, **163**(3), A499–A503, DOI: 10.1149/2.0881603jes.

13 C. Yang, J. Chen, X. Ji, T. P. Pollard, X. Lu, C. J. Sun, S. Hou, Q. Liu, C. Liu, T. Qing, *et al.*, Aqueous Li-ion Battery Enabled by Halogen Conversion-Intercalation Chemistry in Graphite, *Nature*, 2019, **569**(7755), 245–250, DOI: 10.1038/s41586-019-1175-6.

14 Q. Guo, K.-I. Kim, S. Li, A. M. Scida, P. Yu, S. K. Sandstrom, L. Zhang, S. Sun, H. Jiang, Q. Ni, *et al.*, Reversible Insertion of I–Cl Interhalogen in a Graphite Cathode for Aqueous Dual-ion Batteries, *ACS Energy Lett.*, 2021, **6**(2), 459–467, DOI: 10.1021/acsenergylett.0c02575.

15 K.-I. Kim, L. Tang, P. Mirabedini, A. Yokoi, J. M. Muratli, Q. Guo, M. M. Lerner, K. Gotoh, P. A. Greaney, C. Fang, *et al.*, $[LiCl_2]$–Superhalide: A New Charge Carrier for Graphite Cathode of Dual-ion Batteries, *Adv. Funct. Mater.*, 2022, **32**(23), 2112709, DOI: 10.1002/adfm.202112709.

16 Y. Ito, C. Lee, Y. Miyahara, S. Yamazaki, T. Yamada, K. Hiraga, T. Abe and K. Miyazaki, Rechargeable Graphite Fluoride Electrodes Realized by Fluoride Anion Insertion and Deinsertion, *Chem. Mater.*, 2022, **34**(19), 8711–8718, DOI: 10.1021/acs.chemmater.2c01850.

17 Y. Ito, C. Lee, Y. Miyahara, K. Miyazaki and T. Abe, Operando Raman Spectroscopy Insights into the Electrochemical Formation of F-Graphite Intercalation Compounds, *ACS Energy Lett.*, 2024, **9**(4), 1473–1479, DOI: 10.1021/acsenergylett.4c00130.

18 S. Tsujimoto, S. Tomioka, K. Takegoshi, M. Murakami, C. Lee, Y. Miyahara, Y. Shimizu, K. Hiraga, M. Kagawa, K. Miyazaki and T. Abe, Electrochemical Characteristics of Graphite–LiF Composite Electrodes for Lithium-Based Energy Storage Systems, *ACS Electrochem.*, 2025, **1**(12), 2859–2865, DOI: 10.1021/acselectrochem.5c00392.

19 N. Sharma, M. Dubois, K. Guérin, V. Pischedda and S. Radescu, Fluorinated (Nano)Carbons: CF_x Electrodes and CF_x-Based Batteries, *Energy Technol.*, 2021, **9**(4), 2000605, DOI: 10.1002/ente.202000605.

20 W. Liu, S. Ma, B. Wan, Y. Li, R. Guo, C. Wu, S. Ma, H. Pei and J. Xie, Carbon fluorides for rechargeable batteries, *Appl. Mater. Today*, 2023, **33**, 101883, DOI: 10.1016/j.apmt.2023.101883.

21 S. Ko, Y. Yamada and A. Yamada, An Overlooked Issue for High-Voltage Li-ion Batteries: Suppressing the Intercalation of Anions into Conductive Carbon, *Joule*, 2021, **5**(4), 998–1009, DOI: 10.1016/j.joule.2021.02.016.

22 G. Nagasubramanian and M. Rodriguez, Performance Enhancement at Low Temperatures and In Situ X-ray Analyses of Discharge Reaction of Li/$(CF_x)_n$ Cells, *J. Power Sources*, 2007, **170**(1), 179–184, DOI: 10.1016/j.jpowsour.2007.04.023.

23 N. Watanabe, R. Hagiwara, T. Nakajima, H. Touhara and K. Ueno, Solvents Effects on Electrochemical Characteristics Of Graphite Fluoride-Lithium Batteries, *Electrochim. Acta*, 1982, **27**(11), 1615–1619, DOI: 10.1016/0013-4686(82)80088-1.

24 B. Sayahpour, H. Hirsh, S. Bai, N. B. Schorr, N. Lambert, M. Mayer, W. Bao, D. Cheng, M. Zhang, K. Leung, *et al.*, Revisiting Discharge Mechanism of CF_x as a High Energy Density Material for Lithium Primary Battery, *Adv. Energy Mater.*, 2022, **12**, 2103196, DOI: 10.1002/aenm.202103196.

25 Z. Fang, Y. Yang, T. Zheng, N. Wang, C. Wang, X. Dong, Y. Wang and Y. Xia, An All-Climate CF_x/Li Battery with Mechanism-Guided Electrolyte, *Energy Storage Mater.*, 2021, **42**, 477–483, DOI: 10.1016/j.ensm.2021.08.002.

26 N. Watanabe, T. Nakajima and R. Hagiwara, Discharge Reaction and Overpotential of the Graphite Fluoride Cathode in a Nonaqueous Lithium Cell, *J. Power Sources*, 1987, **20**(1–2), 87–92, DOI: 10.1016/0378-7753(87)80095-2.

27 J. Jiang, H. Ji, P. Chen, C. Ouyang, X. Niu, H. Li and L. Wang, The Influence of Electrolyte Concentration and Solvent on Operational Voltage of Li/CF Primary Batteries Elucidated by Nernst Equation, *J. Power Sources*, 2022, **527**, 231193, DOI: 10.1016/j.jpowsour.2022.231193.

28 T. Wu, Y. Cui, K. Wei, C. Lai, Y. Zhao, S. Ni, Y. Chen, X. Gao, Y. Cui and C. Li, Catalysis of Nickel Nanodomains on Li-F Dissociation for High-Capacity Fluoride Cathodes with Prior Delithiation Ability, *Nano Energy*, 2022, **103**(B), 107843, DOI: 10.1016/j.nanoen.2022.107843.

29 S. Ma, W. Liu, D. Zhang, C. Yang, Y. Luo, X. Lou, R. Guo, Y. Wang and J. Xie, Controllable Solvent Treatment of Fluorinated Graphite for High Power Density and Low Cathode Swelling Lithium Primary Batteries, *Chem. Eng. J.*, 2023, **474**, 145819, DOI: 10.1016/j.cej.2023.145819.

30 N. Li and D. Su, In-Situ Structural Characterizations of Electrochemical Intercalation of Graphite Compounds, *Carbon Energy*, 2019, **1**(2), 200–218, DOI: 10.1002/cey2.21.

31 H. Fujimoto, S. Takagi, K. Shimoda, H. Kiuchi, K.-i. Okazaki, T. Murata, Z. Ogumi and T. Abe, Analysis of Intercalation/De-Intercalation of Li Ions Into/From Graphite at 0 °C via Operando Synchrotron X-ray Diffraction, *J. Electrochem. Soc.*, 2021, **168**(9), 090515, DOI: 10.1149/1945-7111/ac2280.

32 F. Li, Y. Li, H. Li, L. Ren, J. Hu, C. Ma, A. Zhu, S. Wu, X. Gu and M. Wu, AlF_3-stabilized cathode electrolyte interphase with superior PF_6^- affinity and PF_6^- -transferred characteristics for dual-ion batteries, *Energy Storage Mater.*, 2025, **80**, 104353, DOI: 10.1016/j.ensm.2025.104353.

33 Y. Zhao, K. Xue and D. Y. W. Yu, Tuning Electrolyte Solvation Structure and CEI Film to Enable Long Lasting FSI−-Based Dual-Ion Battery, *Adv. Funct. Mater.*, 2023, **33**(44), 2300305, DOI: 10.1002/adfm.202300305.

34 K. Zhang, D. Li, J. Shao, Y. Jiang, L. Lv, Q. Shi, Q. Qu and H. Zheng, Electrochemistry-Driven Interphase Doubly Protects Graphite Cathodes for Ultralong Life and Fast Charge of Dual-Ion Batteries, *ChemSusChem*, 2023, **16**, e202300324, DOI: 10.1002/cssc.202300324.

35 X. Han, G. Xu, Z. Zhang, X. Du, P. Han, X. Zhou, G. Cui and L. Chen, An In Situ Interface Reinforcement Strategy Achieving Long Cycle Performance of Dual-Ion Batteries, *Adv. Energy Mater.*, 2019, **9**, 11804022, DOI: 10.1002/aenm.201804022.

36 G. Wang, F. Wang, P. Zhang, J. Zhang, T. Zhang, K. Müllen and X. Feng, Polarity-Switchable Symmetric Graphite Batteries with High Energy and High Power Densities, *Adv. Mater.*, 2018, **30**, e1802949, DOI: 10.1002/adma.201802949.

